SYNTHESIS AND CHARACTERIZATION OF NANOPARTICLE SUSPENSIONS: TOWARDS QUANTITATIVE SURFACE-ENHANCED RAMAN SPECTROSCOPIC SENSING

BY

BRENT M. DEVETTER

THESIS

Submitted in partial fulfillment of the requirements
for the degree of Master of Science in Electrical and Computer Engineering
in the Graduate College of the
University of Illinois at Urbana-Champaign, 2013

Urbana, Illinois

Adviser:

Professor Rohit Bhargava

ABSTRACT

Surface-enhanced Raman spectroscopy (SERS) is an ultrasensitive technique with applications ranging from *in vitro* and *in vivo* biological sensing to chemical and explosives detection. In this thesis, we explore the design and characterization of suspensions of nanoparticles prior to their use for SERS-based molecular sensing. A major problem in SERS-based measurements is that the signals are often not interpreted quantitatively. Measurements performed in suspension mimic the nanoprobe-to-nanoprobe optical interactions expected to be found in tissues with embedded nanoprobes while particle-level measurements of synthesized nanoparticles provide the molecular basis for calculations. We find that careful consideration of the localized surface plasmon resonance of SERS nanoprobes with respect to laser excitation wavelength is essential for maximizing detectable SERS signal. Additionally, the reporter molecule load per particle depends on synthesis conditions and the shape of the nanoparticles. Together, well-characterized suspensions can be used to understand the molecular and electromagnetic aspects of recorded SERS data.

TABLE OF CONTENTS

CHAPTER 1

INTRODUCTION TO SURFACE-ENHANCED RAMAN SPECTROSCOPY AND PLASMONICS

1.1 Introduction

The development of advanced imaging diagnostics is essential for the accurate and rapid identification of cancerous tissues. Today, a pressing challenge in the medical and scientific communities is the availability of imaging technologies that offer both high sensitivity and chemical specificity. With the assistance of rationally designed nanoprobes, these requirements may be fulfilled through an optical spectroscopic technique called surface-enhanced Raman spectroscopy (SERS). Raman spectroscopy was first discovered between 1922 and 1927 by Sir C.V. Raman. Sir Raman distinguished between Rayleigh scattering and a weak secondary scattering phenomenon which he discovered by using colored filters and samples illuminated under sunlight.[1] Named after Sir Raman, Raman scattering is an inelastic light scattering process from which the molecular composition of analytes may be obtained. Fluorescence spectroscopy has historically been preferred over Raman spectroscopy because fluorescent dye molecules have cross-sections roughly 10^{14} orders of magnitude greater than that of Raman scattering cross-sections.[2–4] As a result, Raman spectroscopy's inherently weak signal limited its widespread use until the 1970s when SERS was first discovered. In 1974, Fleischmann and coworkers discovered that pyridine adsorbed on roughened silver electrodes significantly increased the detected Raman scattered light.[5] Jeanmaire and Van Duyne further explained Fleischmann's observation in 1977 with an electromagnetic description.[6] In 1997, Nie and Emory published a report in *Science* describing Raman scattering sensitivities down to single-molecule detection limits and helped to ignite a renewed interest in SERS.[2] Furthermore, with recent advances in

nanofabrication and nanosynthesis, applications and interest in SERS nanoprobes have exponentially increased.[7]

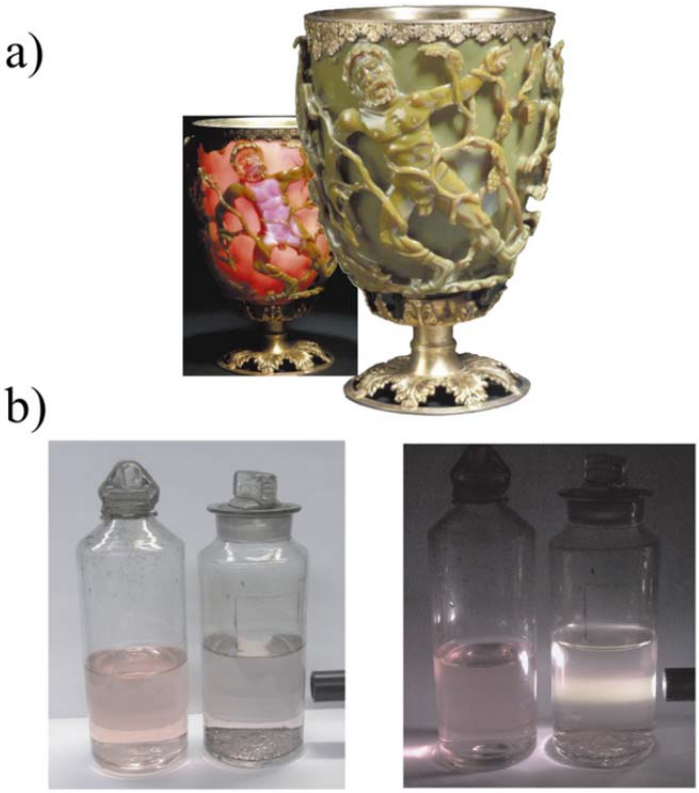

Figure 1. (a) The Roman-era Lycurgus Cup (c. 4th century CE) with glass-embedded nanoscale gold particles. When illuminated directly, the cup appears red as a result of nanoscale gold's optical properties.[8] (b) Faraday's colloidal gold solutions. On the left of each photograph is a false pink solution meant to resemble colloidal gold. On the right of each photograph is a colloidal gold solution.[9]

At least since the 4th century CE, we have known that noble metals (gold, copper, or silver) can have brilliant optical properties. As shown in Figure 1(a), the Roman-era Lycurgus Cup, consisting of colloidal gold embedded within glass, appears red when illuminated from the inside and green when illuminated indirectly. Furthermore, one of the first scientific inquiries into the characteristics of noble metals was initiated by Michael Faraday in 1856. Faraday synthesized gold colloids (Figure 1(b)) via the reduction of gold chloride with phosphorous and studied their optical properties. He found that his solutions appeared red which, of course, are

dissimilar to that of bulk gold.[9] As shown, the light scattering properties of colloidal suspensions are distinct from that of solutions containing dye.

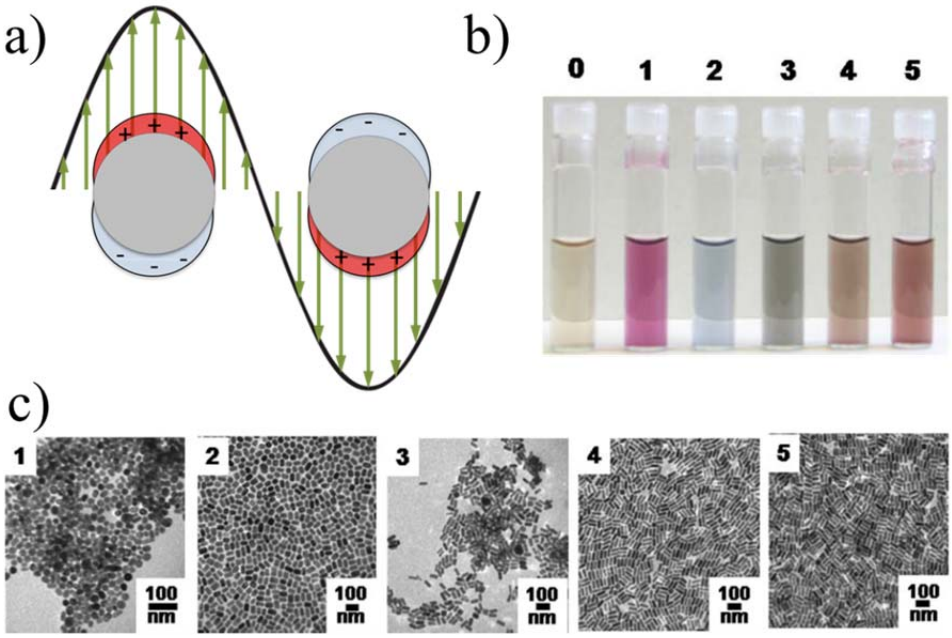

Figure 2. (a) Noble metal nanoparticles interact with light and generate localized surface plasmon resonances. Surface plasmons are the collective oscillation of conduction electrons that propagate on the surface of roughened metal substrates or nanoscale metals. (b) Gold nanorods have tunable plasmon resonances that are dependent on their aspect ratio. (c) Transmission electron micrographs of varying aspect ratio gold nanorods.[10]

Why does colloidal gold appear red? Surface conduction electrons in noble metal nanoparticles collectively oscillate resulting in the generation of localized surface plasmons (Figure 2(a)). This light-matter interaction results in strongly absorbing particles, typically within the visible or near-infrared spectrum for gold or silver nanoparticles. Colloidal gold, consisting of gold nanospheres, absorbs green light (~ 520 nm) resulting in a reddish appearance. The optical properties of gold nanoparticles are further tunable by altering components such as size, shape, or composition. Figure 2 shows the optical characteristics of varying aspect ratio gold nanorods.

Engineering the optical properties of noble metal nanoprobes can significantly increase the Raman scattering cross-section of analytes. There are two mechanisms that explain surface-enhancement. The first and more subtle effect is chemical enhancement. Chemical enhancement arises from the resonance of the molecule bound to a substrate or nanoparticle.[11] Because chemical enhancement is molecule dependent, researchers typically neglect this effect and focus on the second and more controllable mechanism. The second mechanism is called electromagnetic enhancement[12] and may be described in terms of the evanescent fields generated by the propagation of surface plasmons. Analytes within this field are surface-enhanced and, subsequently, have an increased Raman scattering cross-section.

Researchers have demonstrated a wide variety of SERS applications ranging from *in vivo* biological sensing[13,14] to pesticide detection[15] and glucose sensors for diabetics.[16] Furthermore, SERS substrates are excellent candidates for highly sensitive chemical biosensors[17,18] using techniques such as nanosphere lithography.[19] Substrates, however, are limited in terms of their applicability to tissue and *in vivo*-based measurements. Here, we focus on the rational design, synthesis, and characterization of in-suspension nanoparticles for biological applications.

1.2 Electromagnetic Theory of Surface-Enhanced Raman Spectroscopy

As a limiting condition, we consider only the electromagnetic mechanism of SERS for the design of nanoprobes. Electromagnetic enhancement is well described by classical electrodynamics,[20] whereas chemical enhancement remains an active area of research with experimental and theoretical reports debating its origins and relative contribution to overall enhancement.[11,21,22]

Understanding the optical properties of noble metals is essential for designing highly efficient nanoprobes. Noble metals may be mathematically described by the Drude model in which electron motion is analogous to a bound, damped harmonic oscillator. Comparison with experimentally measured optical constants match well with calculated constants in the visible and near-infrared regions.[23] Experimentally obtained optical constants of thin metals are available from Palik[24] and Johnson and Christy.[25] A modified form of the Drude model with incident light E_0 may be represented by the following partial differential equation:

$$m\frac{\partial^2 x}{\partial t^2} + m\gamma\frac{\partial x}{\partial t} + m\omega_0^2 x = -eE_0 e^{-i\omega_0 t} \tag{1.1}$$

where e is the charge of an electron, m is the effective mass of the electrons, γ is the damping constant which accounts for electron radiative damping, and $m{\omega_0}^2$ describes the stiffness of the bound electrons. Under the assumption of a linear response, Equation (1.1) may be solved for x(t) and, subsequently, the permittivity. For a given plasma frequency ${\omega_p}^2$ of a material, the permittivity of the metal is represented by the following:

$$\varepsilon(\omega) = 1 + \frac{\omega_p^2}{\omega_0^2 - \omega^2 - i\omega\gamma} \tag{1.2}$$

Raman-active molecules placed near the surface of noble metal nanoprobes are surface-enhanced due to the evanescent field generated through the oscillation of plasmons on the nanoparticle surface. A simple model for elucidating the electromagnetic enhancement mechanism of SERS may be developed by investigating spherical scattering of metallic nanospheres where molecules act as electric dipoles.[26] A generalized electromagnetic theory of spherical scattering for arbitrarily sized spheres and optical properties was first developed by

Mie in 1908.[27] A sphere of radius *a* has size parameter $x = \frac{2\pi a}{\lambda} n_{media}$. Given a wavevector $k = 2\pi n_{media} / \lambda_0$, the Mie coefficients a_n and b_n are defined as the following:[28]

$$a_n = \frac{m\psi_n(mx)\psi_n'(x) - \psi_n(x)\psi_n'(mx)}{m\psi_n(mx)\xi_n'(x) - \xi_n(x)\psi_n'(mx)}$$
$$b_n = \frac{\psi_n(mx)\psi_n'(x) - m\psi_n(x)\psi_n'(mx)}{\psi_n(mx)\xi_n'(x) - m\xi_n(x)\psi_n'(mx)} \quad (1.3)$$

The ratio of indices of refraction *m* are defined as $m = n_{metal} / n_{media}$. Riccati-Bessel functions are described by: $\psi_n(\rho) = \rho j_n(\rho)$ and $\zeta_n(\rho) = \rho h_n^1(\rho)$. The extinction (scattering plus absorption) of light is calculated from the Mie coefficients. In particular, the extinction cross section C_{ext} is defined as the following:[28]

$$C_{ext} = \frac{2\pi}{k^2} \sum_{n=1}^{\infty} (2n+1) \, \mathrm{Re}\{a_n + b_n\} \quad (1.4)$$

Similarly, the scattering cross section is defined as:

$$C_{sca} = \frac{2\pi}{k^2} \sum_{n=1}^{\infty} (2n+1)(|a_n|^2 + |b_n|^2) \quad (1.5)$$

The absorption cross section is calculated as: $C_{abs} = C_{ext} - C_{sca}$. For rapid calculation and a more intuitive sense of cross sections, a quasistatic approach may be taken in which the electric field over the surface of the particle is assumed constant. Note that this approximation is only valid for particles much smaller than the wavelength of incident light:[28]

$$C_{ext} = \pi a^2 4x \, \mathrm{Im}\left\{ \frac{\varepsilon_{np} - \varepsilon_{media}}{\varepsilon_{np} + 2\varepsilon_{media}} \right\} \quad (1.6)$$

$$C_{sca} = \pi a^2 \frac{8}{3} x^4 \left| \frac{\varepsilon_{np} - \varepsilon_{media}}{\varepsilon_{np} + 2\varepsilon_{media}} \right|^2 \quad (1.7)$$

where ε_{np} and ε_{media} are the dielectric constants of the nanoprobes and the surrounding media, respectively. The term $\frac{\varepsilon_{np} - \varepsilon_{media}}{\varepsilon_{np} + 2\varepsilon_{media}}$ is called the Clausius–Mossotti relation and provides insight as to why noble metals such as gold and silver are excellent plasmonic materials. If ε_{np} begins to approach $-2\varepsilon_{media}$, the absorption and scattering cross-sections of the nanoprobe begin to significantly increase. Fortuitously, gold and silver have negative permittivities in the visible spectrum with minimal losses and, subsequently, excellent plasmonic properties.

Mie theory is an extremely powerful analytical model for the scattering characteristics of spherical particles. However, many experimentally synthesized nanostructures lack spherically symmetric geometries. With recent advances in computing power and algorithm development, a variety of computational tools are available for estimating the electromagnetic enhancement of nonspherical particles.[29] The finite-element method (FEM),[30] finite difference time domain method (FDTD),[31] and the discrete dipole approximation (DDA)[32] have been used extensively in SERS research.

Biomedical researchers are particularly interested in quantifying the nanoprobe's ability to increase the Raman scattering cross-section of molecules. Neglecting chemical enhancement effects, enhancement may be characterized by G, the electromagnetic enhancement factor:[21]

$$G = |E(\lambda_{inc})|^2 |E(\lambda_{inc} + \delta\lambda)|^2 \approx |E(\lambda_{inc})|^4$$

where we assume the Stokes-shifted intensity is on the same order of magnitude as that of the incident field intensity $(\delta\lambda = 0)$.[20] The Raman signature of molecules is enhanced by both the

incident light intensity as well as the scattered light intensity, resulting in an $|E|^4$ dependence. Therefore, highly sensitive SERS-based nanoprobes may be designed through direct application of electromagnetic theory.

1.3 Rationally Designed Nanoprobes

Gold has a long history of medicinal uses. Beginning in 1927 researchers used gold thioglucose to treat rheumatoid arthritis.[33] Nanoscale gold is chemically inert, has low cytotoxicity,[34] and has been successfully used in numerous short-term *in vivo* studies.[13,14] In contrast to other nanomaterials such as cadmium selenide quantum dots[35,36] and nanoscale silver,[37] gold's use in biological systems is well-established and less controversial.

Our ability to fabricate and synthesize inorganic nanostructures has grown tremendously in recent years. In 1857, Faraday prepared colloidal gold using phosphorous to reduce gold chloride.[9] In the 1950s, Turkevich and coworkers developed a method in which trisodium citrate reduced a boiling solution of chloroauric acid.[38] Today, wet chemical synthesis of anisotropic nanostructures such as hollow gold nanospheres,[39] gold/silver nanocages,[40] and gold nanorods[41] are routinely performed in labs across the world. Anisotropic nanostructures are typically straightforward to synthesize with a minimal amount of reagents and specialized equipment. For example, hollow gold nanospheres are synthesized via a sacrificial cobalt nanosphere template. After gold is deposited onto a cobalt surface, the cobalt is etched away, resulting in a hollow cavity. Similarly, gold/silver nanocages are formed through the galvanic replacement of gold on silver nanocubes. Template-based techniques such as these require careful attention to stoichiometry but are generally reproducible and facile synthetic methods. Low-aspect ratio gold nanorods are formed from a seed-mediated process in which a crystal growth directing

surfactant, cetyltrimethylammonium bromide (CTAB), is added to a growth solution consisting of silver impurity ions and chloroauric acid. Nanoprobe design is accomplished through a consideration of fabrication and synthetic capabilities in combination with electromagnetic computation. Additional parameters to consider are the optical environment in which the nanoprobes will be embedded, cellular uptake, and toxicity. Here, we are primarily concerned with optimizing size and geometry for obtaining maximal signal.

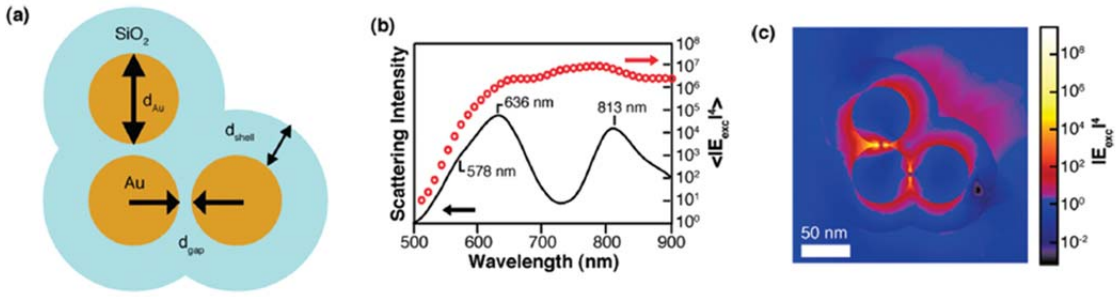

Figure 3. (a) Trimer nanostructure in which three gold nanoprobes are placed next to each other and encapsulated in silica. (b) Scattering intensity profile of trimer structure. (c) FEM simulation of electromagnetic enhancement ($|E|^4$) of trimer structure at 633 nm excitation.[42]

Concentration of optical fields in the near-field is accomplished through nanoscale features with high radii of curvature or interplasmonic coupling between metallic surfaces. Edges and corners with high radii of curvature are described by the so-called "lightning rod" effect of SERS.[43] This effect is generally well-understood from a classical perspective, but it remains challenging to explore experimentally because chemical techniques tend not to produce atomically defined edges. The second and more common technique is to design nanoprobes through interplasmonic coupling. As shown in Figure 3, gold nanoprobes placed in trimer configurations strongly couple. Configurations such as these are called controlled aggregates. A

variety of reports have demonstrated that aggregates in solution offer several orders of magnitude enhancement over monodisperse nanoprobes.[44–46] Nonetheless, these techniques tend to be unreliable and lead to the formation of "hot-spots." Hot-spots are particularly difficult to control for in-suspension measurements and lead to results with poor reproducibility.

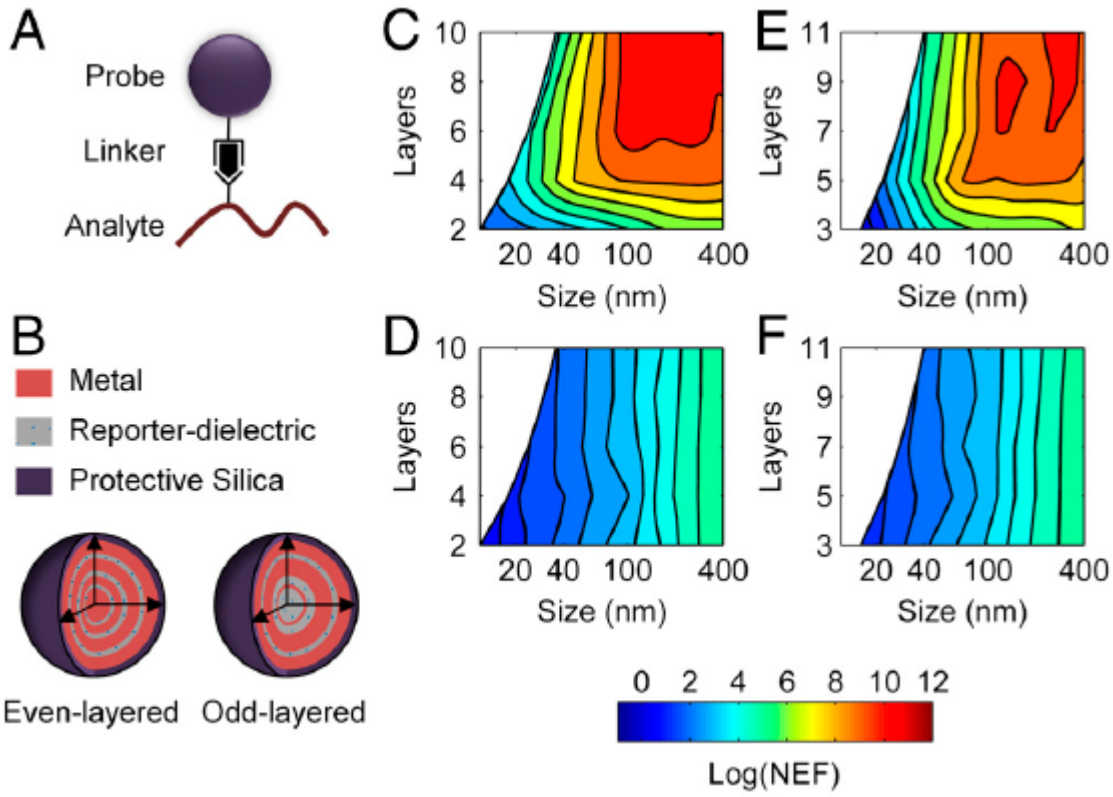

Figure 4. (a) Nanoprobe structure with attached analyte. (b) Internal structure with alternating layers of metal-dielectric material. At 785 nm laser excitation, net enhancement factor (NEF) of (c) even and (e) odd layers of silver-silica. The NEF arises from a ratio between the electromagnetic enhancement to a single Raman-active molecule. (d) and (f) are the numerical enhancement values in the absence of SERS.[47]

An alternative approach to hot-spots is the design of multilayered metal-dielectric shells. Recently, our group has demonstrated electromagnetic enhancements approaching single-molecule sensitivities may be achieved through spherically symmetric alternating shells of silver-silica.[47] As shown in Figure 4, certain configurations with 4 layers or more can yield

enhancement factors greater than 10^8 orders of magnitude. In 2011, Lim and coworkers experimentally demonstrated a realization of this model using DNA-modified gold nanoparticles to produce gold-gap-gold nanospheres.[48] Due to the practical complexities of large-scale synthesis of multilayered nanostructures, single-molecule sensitivities have yet to be achieved.

Preparation of nanoprobes with targeting and SERS capabilities encompass a variety of diverse surface modification techniques. SERS-active molecules are typically electrostatically bound to the nanoprobe surface and encapsulated in high molecular weight (~5,000-10,000 g/mol) poly(ethylene glycol).[13,49] Alternatively, a silica shell may be grown around the metallic core to protect and trap bound molecules.[14] Silica growth is typically achieved in organic solvents using active silica reagents.[50] A completely aqueous phase method to encapsulate and trap SERS-active molecules is layer-by-layer polyelectrolyte coating in which charged polymers wrap around the nanoprobe.[51] Targeting capabilities are generally achieved through the addition of reactive moieties such as carboxylic acid or amine to the nanoprobe surface. Commonly, poly(ethylene glycol) encapsulated nanoprobes are terminated with –COOH and react readily in aqueous solution with 1-ethyl-3-(3-dimethylaminopropyl)carbodiimide (EDC) and N-hydroxysulfosuccinimide (sulfo-NHS) to form an amide linkage between the nanoprobe and amine-bearing protein.

As discussed in Chapter 2, a final consideration for rational nanoprobe design is nanoprobe-to-nanoprobe optical interactions. A relationship between SERS intensity and localized surface plasmon resonance exists for in-suspension measurements. Mathematically, this may be modeled as enhancement modified with Beer's law. When light propagates through a path length of nanoprobes or tissue with embedded nanoprobes, nanoprobe scattering and absorption (extinction) can significantly impact measurable signal.

1.4 SERS and Plasmonics Applications

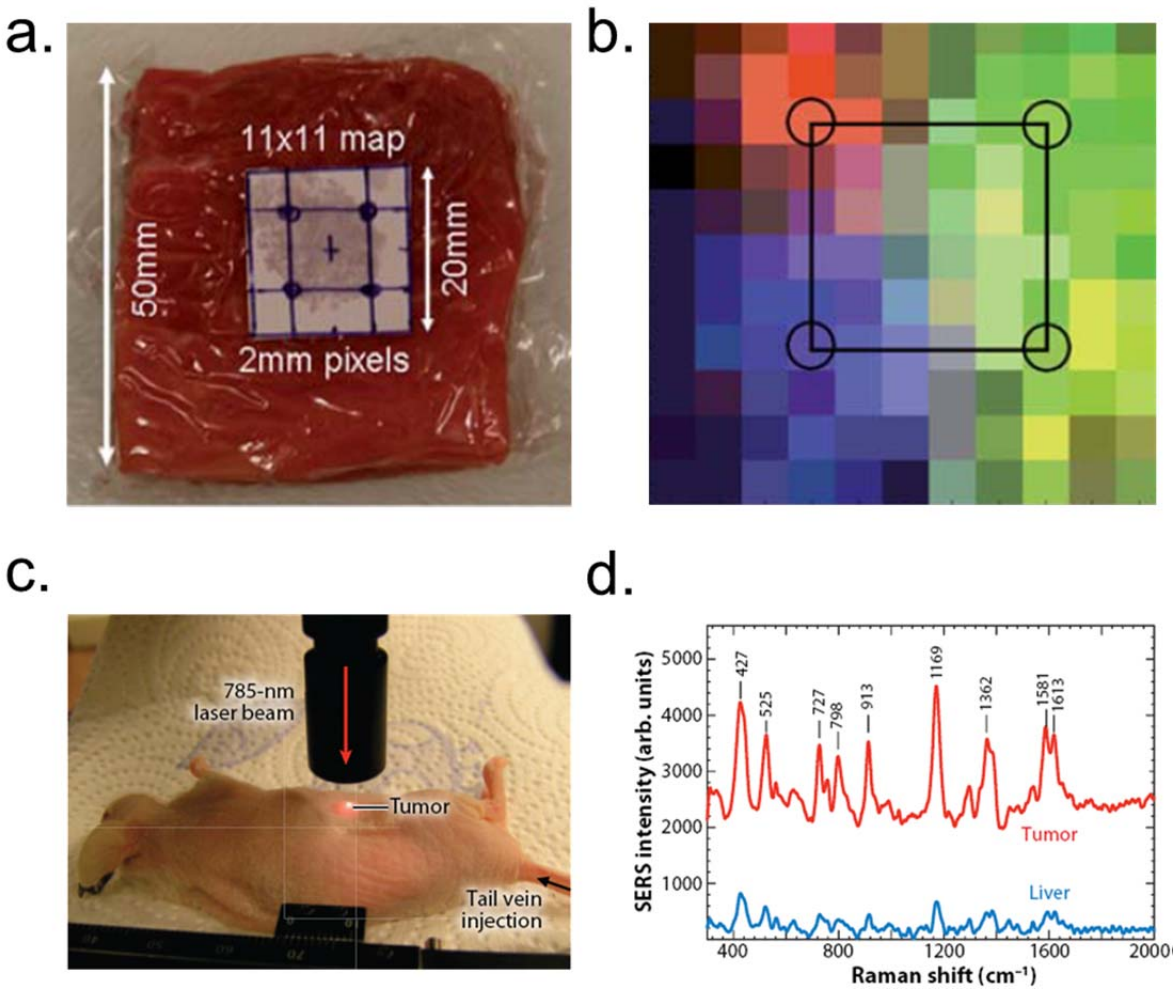

Figure 5. (a) Porcine tissue with four injection points. Nanoprobes with different Raman signatures were embedded within the tissue. (b) Multiplexed image of nanoprobes demonstrating the capability to distinguish between nanoprobes in tissue environments.[52] (c) Photograph of nude mouse bearing a human head-and-neck (Tu686) tumor. Nanoprobes were injected into the bloodstream through a tail vein injection. (d) SERS spectra of the liver and tumor with accumulated nanoprobes.[13]

SERS is on the cusp of becoming a widely utilized technology in numerous fields such as medical diagnostics and chemical and biological sensing. In contrast to fluorescence, SERS nanoprobes are able to distinguish between a virtually limitless number of analytes.[14,47] In tissue applications, this is particularly useful because researchers are continually identifying new

biomarkers.[53,54] In Figure5, researchers have demonstrated the ability to multiplex SERS nanoprobes in tissue samples as well as distinguish between healthy tissue and nanoprobe loaded tumors *in vivo.*

More generally, plasmonic materials have found a variety of exciting applications in recent years. Stipe and coworkers developed a data storage device based on plasmonic gold nanoantennas.[55] Ultrasensitive colorimetric protein sensors based on gold nanoparticles have been developed to eliminate the need for fluorometers or other expensive equipment.[56] Developing countries may find sensors such as these to be a vital component of low-cost diagnostics. Photonics researchers have also found plasmonic materials useful for developing and designing new detectors and lasers.[57] This field will continue to flourish as new technologies and devices are developed and commercialized.

1.5 Thesis Scope and Organization

The aim of this work is to contribute to the body of knowledge in the design, fabrication, and biological applications of SERS nanoprobes. To date there have been numerous scientific reports on the possibilities of SERS for *in vitro* and *in vivo* sensing. Nonetheless, these reports have yet to fully describe and investigate the necessity for considering the optical properties of colloidal suspensions of nanoprobes. Nanoprobes embedded within tissue will inherently scatter and absorb light due to nanoprobe-to-nanoprobe light interaction. In this thesis, we explore how to minimize this effect by tuning the optical characteristics of gold nanoprobes.

Chapter 1 has provided background information the theory and applications of surface-enhanced Raman spectroscopy. Chapter 2 investigates the optical characteristics of varying concentrations of gold nanospheres with electrostatically bound Raman reporters. A model is developed to explain the extinction of light through a finite path length of gold nanoprobe

suspensions. In Chapter 3, edge and corner effects are investigated for colloidal suspensions. We determine the effect of geometry on measured SERS intensity. Finally, Chapter 4 concludes with an outlook and future work.

1.6 References

1. Raman, C. V.; Krishnan, K. S. A New Type of Secondary Radiation. *Nature* **1928**, *121*, 501.
2. Nie, S.; Emory, S. R. Probing Single Molecules and Single Nanoparticles by Surface-Enhanced Raman Scattering. *Science* **1997**, *275*, 1102–1106.
3. Introduction to Fluorescence. In *Principles of Fluorescence Spectroscopy*; Lakowicz, J. R., Ed.; Springer US, 2006; pp. 1–26.
4. Cohen, B. E. Biological Imaging: Beyond Fluorescence. *Nature* **2010**, *467*, 407–408.
5. Fleischmann, M.; Hendra, P. J.; McQuillan, A. J. Raman Spectra of Pyridine Adsorbed at a Silver Electrode. *Chemical Physics Letters* **1974**, *26*, 163–166.
6. Jeanmaire, D. L.; Van Duyne, R. P. Surface Raman Spectroelectrochemistry: Part I. Heterocyclic, Aromatic, and Aliphatic Amines Adsorbed on the Anodized Silver Electrode. *Journal of Electroanalytical Chemistry and Interfacial Electrochemistry* **1977**, *84*, 1–20.
7. Sharma, B.; Frontiera, R. R.; Henry, A.-I.; Ringe, E.; Van Duyne, R. P. SERS: Materials, Applications, and the Future. *Materials Today* **2012**, *15*, 16–25.
8. Wagner, F. E.; Haslbeck, S.; Stievano, L.; Calogero, S.; Pankhurst, Q. A.; Martinek, K.-P. Before Striking Gold in Gold-ruby Glass. *Nature* **2000**, *407*, 691–692.
9. Discovering Discovery: How Faraday Found the First Metallic Colloid http://www.academia.edu/442267/Discovering_Discovery_How_Faraday_Found_the_First_Metallic_Colloid (accessed Jan 22, 2013).
10. Murphy, C. J.; Gole, A. M.; Hunyadi, S. E.; Stone, J. W.; Sisco, P. N.; Alkilany, A.; Kinard, B. E.; Hankins, P. Chemical Sensing and Imaging with Metallic Nanorods. *Chem. Commun.* **2008**, 544–557.
11. Wu, D.-Y.; Liu, X.-M.; Duan, S.; Xu, X.; Ren, B.; Lin, S.-H.; Tian, Z.-Q. Chemical Enhancement Effects in SERS Spectra: A Quantum Chemical Study of Pyridine Interacting with Copper, Silver, Gold and Platinum Metals. *J. Phys. Chem. C* **2008**, *112*, 4195–4204.
12. Xu, H.; Aizpurua, J.; Käll, M.; Apell, P. Electromagnetic Contributions to Single-molecule Sensitivity in Surface-enhanced Raman Scattering. *Phys. Rev. E* **2000**, *62*, 4318–4324.
13. Qian, X.; Peng, X.-H.; Ansari, D. O.; Yin-Goen, Q.; Chen, G. Z.; Shin, D. M.; Yang, L.; Young, A. N.; Wang, M. D.; Nie, S. In Vivo Tumor Targeting and Spectroscopic Detection with Surface-enhanced Raman Nanoparticle Tags. *Nat Biotech* **2008**, *26*, 83–90.
14. Zavaleta, C. L.; Smith, B. R.; Walton, I.; Doering, W.; Davis, G.; Shojaei, B.; Natan, M. J.; Gambhir, S. S. Multiplexed Imaging of Surface Enhanced Raman Scattering Nanotags in Living Mice Using Noninvasive Raman Spectroscopy. *Proceedings of the National Academy of Sciences* **2009**, *106*, 13511 –13516.
15. Li, J. F.; Huang, Y. F.; Ding, Y.; Yang, Z. L.; Li, S. B.; Zhou, X. S.; Fan, F. R.; Zhang, W.; Zhou, Z. Y.; Wu, D. Y. *et al.* Shell-isolated Nanoparticle-enhanced Raman Spectroscopy. *Nature* **2010**, *464*, 392–395.

16. Ma, K.; Yuen, J. M.; Shah, N. C.; Walsh, J. T., Jr; Glucksberg, M. R.; Van Duyne, R. P. In Vivo, Transcutaneous Glucose Sensing Using Surface-enhanced Spatially Offset Raman Spectroscopy: Multiple Rats, Improved Hypoglycemic Accuracy, Low Incident Power, and Continuous Monitoring for Greater Than 17 Days. *Anal. Chem.* **2011**, *83*, 9146–9152.
17. Zhang, X.; Yonzon, C. R.; Young, M. A.; Stuart, D. A.; Van Duyne, R. P. Surface-enhanced Raman Spectroscopy Biosensors: Excitation Spectroscopy for Optimisation of Substrates Fabricated by Nanosphere Lithography. *IEE Proc Nanobiotechnol* **2005**, *152*, 195–206.
18. Vo-Dinh, T.; Wang, H.; Scaffidi, J. Plasmonic Nanoprobes for SERS Biosensing and Bioimaging. *Journal of Biophotonics* **2010**, *3*, 89–102.
19. Hulteen, J. C.; Van Duyne, R. P. Nanosphere Lithography: A Materials General Fabrication Process for Periodic Particle Array Surfaces. *Journal of Vacuum Science & Technology A: Vacuum, Surfaces, and Films* **1995**, *13*, 1553–1558.
20. Schatz, G. C.; Van Duyne, R. P. *Electromagnetic Mechanism of Surface-enhanced Spectroscopy*; Wiley, 2002; Vol. Volume 1 Theory and Instrumentation.
21. Xu, H.; Wang, X.-H.; Persson, M. P.; Xu, H. Q.; Käll, M.; Johansson, P. Unified Treatment of Fluorescence and Raman Scattering Processes Near Metal Surfaces. *Phys. Rev. Lett.* **2004**, *93*, 243002.
22. Maitani, M. M.; Ohlberg, D. A. A.; Li, Z.; Allara, D. L.; Stewart, D. R.; Williams, R. S. Study of SERS Chemical Enhancement Factors Using Buffer Layer Assisted Growth of Metal Nanoparticles on Self-Assembled Monolayers. *J. Am. Chem. Soc.* **2009**, *131*, 6310–6311.
23. Novotny, L.; Hecht, B. *Principles of Nano-Optics*; Reissue.; Cambridge University Press, 2011.
24. Palik, E. D. *Handbook of Optical Constants of Solids: Index*; Academic Press, 1998.
25. Johnson, P. B.; Christy, R. W. Optical Constants of the Noble Metals. *Phys. Rev. B* **1972**, *6*, 4370–4379.
26. Kerker, M.; Wang, D.-S.; Chew, H. Surface Enhanced Raman Scattering (SERS) by Molecules Adsorbed at Spherical Particles: Errata. *Appl. Opt.* **1980**, *19*, 4159–4174.
27. Mie, G. Beiträge Zur Optik Trüber Medien, Speziell Kolloidaler Metallösungen. *Annalen der Physik* **1908**, *330*, 377–445.
28. Bohren, C. F.; Huffman, D. R. *Absorption and Scattering of Light by Small Particles*; 2007.
29. Kahnert, F. M. Numerical Methods in Electromagnetic Scattering Theory. *Journal of Quantitative Spectroscopy and Radiative Transfer 79–80*, 775–824.
30. Khoury, C. G.; Norton, S. J.; Vo-Dinh, T. Plasmonics of 3-D Nanoshell Dimers Using Multipole Expansion and Finite Element Method. *ACS Nano* **2009**, *3*, 2776–2788.
31. Zhao, J.; Pinchuk, A. O.; McMahon, J. M.; Li, S.; Ausman, L. K.; Atkinson, A. L.; Schatz, G. C. Methods for Describing the Electromagnetic Properties of Silver and Gold Nanoparticles. *Acc. Chem. Res.* **2008**, *41*, 1710–1720.
32. Jain, P. K.; Lee, K. S.; El-Sayed, I. H.; El-Sayed, M. A. Calculated Absorption and Scattering Properties of Gold Nanoparticles of Different Size, Shape, and Composition: Applications in Biological Imaging and Biomedicine. *J. Phys. Chem. B* **2006**, *110*, 7238–7248.
33. Laude, D. Die Gunstige Beeinflussung Schichender Dauerinfekte Durch Solganal. *Much. Med. Wochenschr* **1927**, 1132.
34. Alkilany, A. M.; Murphy, C. J. Toxicity and Cellular Uptake of Gold Nanoparticles: What We Have Learned so Far? *J. Nanopart. Res.* **2010**, *12*, 2313–2333.

35. Tsoi, K. M.; Dai, Q.; Alman, B. A.; Chan, W. C. W. Are Quantum Dots Toxic? Exploring the Discrepancy Between Cell Culture and Animal Studies. *Acc. Chem. Res.* **2012**.
36. Chou, L. Y. T.; Chan, W. C. W. Nanotoxicology: No Signs of Illness. *Nature Nanotechnology* **2012**, *7*, 416–417.
37. Hansen, S. F.; Baun, A. When Enough Is Enough. *Nature Nanotechnology* **2012**, *7*, 409–411.
38. Turkevich, J.; Stevenson, P. C.; Hillier, J. A Study of the Nucleation and Growth Processes in the Synthesis of Colloidal Gold. *Discuss. Faraday Soc.* **1951**, *11*, 55–75.
39. Schwartzberg, A. M.; Olson, T. Y.; Talley, C. E.; Zhang, J. Z. Synthesis, Characterization, and Tunable Optical Properties of Hollow Gold Nanospheres. *J Phys Chem B* **2006**, *110*, 19935–19944.
40. Sun, Y.; Xia, Y. Shape-Controlled Synthesis of Gold and Silver Nanoparticles. *Science* **2002**, *298*, 2176–2179.
41. Link, S.; El-Sayed, M. A. Spectral Properties and Relaxation Dynamics of Surface Plasmon Electronic Oscillations in Gold and Silver Nanodots and Nanorods. *J. Phys. Chem. B* **1999**, *103*, 8410–8426.
42. Wustholz, K. L.; Henry, A.-I.; McMahon, J. M.; Freeman, R. G.; Valley, N.; Piotti, M. E.; Natan, M. J.; Schatz, G. C.; Van Duyne, R. P. Structure−Activity Relationships in Gold Nanoparticle Dimers and Trimers for Surface-Enhanced Raman Spectroscopy. *J. Am. Chem. Soc.* **2010**, *132*, 10903–10910.
43. Liao, P. F.; Wokaun, A. Lightning Rod Effect in Surface Enhanced Raman Scattering. *The Journal of Chemical Physics* **1982**, *76*, 751–752.
44. Kelly, K. L.; Lazarides, A. A.; Schatz, G. C. Computational electromagnetics of metal nanoparticles and their aggregates. *Computing in Science & Engineering* **2001**, *3*, 67–73.
45. Bell, S. E. J.; McCourt, M. R. SERS Enhancement by Aggregated Au Colloids: Effect of Particle Size. *Phys. Chem. Chem. Phys.* **2009**, *11*, 7455–7462.
46. Xie, H.; Larmour, I. A.; Smith, W. E.; Faulds, K.; Graham, D. Surface-Enhanced Raman Scattering Investigation of Hollow Gold Nanospheres. *J. Phys. Chem. C* **2012**, *116*, 8338–8342.
47. Kodali, A. K.; Llora, X.; Bhargava, R. Optimally Designed Nanolayered Metal-dielectric Particles as Probes for Massively Multiplexed and Ultrasensitive Molecular Assays. *Proceedings of the National Academy of Sciences* **2010**, *107*, 13620 –13625.
48. Lim, D.-K.; Jeon, K.-S.; Hwang, J.-H.; Kim, H.; Kwon, S.; Suh, Y. D.; Nam, J.-M. Highly Uniform and Reproducible Surface-enhanced Raman Scattering from DNA-tailorable Nanoparticles with 1-nm Interior Gap. *Nat. Nano* **2011**, *6*, 452–460.
49. Jokerst, J. V.; Lobovkina, T.; Zare, R. N.; Gambhir, S. S. Nanoparticle PEGylation for Imaging and Therapy. *Nanomedicine (Lond)* **2011**, *6*, 715–728.
50. Fernández-López, C.; Mateo-Mateo, C.; Álvarez-Puebla, R. A.; Pérez-Juste, J.; Pastoriza-Santos, I.; Liz-Marzán, L. M. Highly Controlled Silica Coating of PEG-Capped Metal Nanoparticles and Preparation of SERS-Encoded Particles†. *Langmuir* **2009**, *25*, 13894–13899.
51. Gole, A.; Murphy, C. J. Polyelectrolyte-Coated Gold Nanorods: Synthesis, Characterization and Immobilization. *Chem. Mater.* **2005**, *17*, 1325–1330.
52. Stone, N.; Kerssens, M.; Lloyd, G. R.; Faulds, K.; Graham, D.; Matousek, P. Surface Enhanced Spatially Offset Raman Spectroscopic (SESORS) Imaging – the Next Dimension. *Chem. Sci.* **2011**, *2*, 776–780.

53. Whitfield, M. L.; George, L. K.; Grant, G. D.; Perou, C. M. Common Markers of Proliferation. *Nat Rev Cancer* **2006**, *6*, 99–106.
54. Sawyers, C. L. The Cancer Biomarker Problem. *Nature* **2008**, *452*, 548–552.
55. Stipe, B. C.; Strand, T. C.; Poon, C. C.; Balamane, H.; Boone, T. D.; Katine, J. A.; Li, J.-L.; Rawat, V.; Nemoto, H.; Hirotsune, A. *et al.* Magnetic Recording at 1.5 Pb M|[minus]|2 Using an Integrated Plasmonic Antenna. *Nature Photonics* **2010**, *4*, 484–488.
56. Rica, R. de la; Stevens, M. M. Plasmonic ELISA for the Ultrasensitive Detection of Disease Biomarkers with the Naked Eye. *Nature Nanotechnology* **2012**, *7*, 821–824.
57. Cho, C.-H.; Aspetti, C. O.; Turk, M. E.; Kikkawa, J. M.; Nam, S.-W.; Agarwal, R. Tailoring Hot-exciton Emission and Lifetimes in Semiconducting Nanowires via Whispering-gallery Nanocavity Plasmons. *Nature Materials* **2011**, *10*, 669–675.

CHAPTER 2

COMPETITION BETWEEN EXTINCTION AND ENHANCEMENT IN SURFACE-ENHANCED RAMAN SPECTROSCOPY

2.1 Introduction

Several methods for using surface-enhanced Raman scattering (SERS)[1] have emerged for biomedical applications including ultrasensitive sensing and multiplexed assays. In particular, nanoparticles have been the focus of recent efforts towards *in vitro* and *in vivo* molecular sensing.[2–4] Nanoparticles can dramatically increase the electric field intensity near and at their surface, providing useful SERS-based probes, especially for deep tissue imaging at varying concentrations.[5] Typically, a nanostructured particle is bioconjugated and employed in the same manner that conventional fluorescent probes are used for molecular imaging. SERS probes are postulated to offer bright and stable signals and extensive multiplexing,[6] while it has been assumed that experimental best practice parallels that of fluorescent probes, i.e. that one should excite at the strongest resonance and use a high concentration. Thus far, the design of nanoparticle-based SERS experiments has focused on maximizing the local electromagnetic field enhancement in or around an individual particle.[7,8] This strategy fails to take into account the physics of propagation in the bulk medium where the same processes which give rise to enhancement also lead to increased extinction of both the illumination and the Raman scattered light.

Reproduced from van Dijk, T., Sivapalan, S.T., DeVetter, B.M., Schulmerich, M.V., Murphy, C.J., Bhargava, R., Carney, P.S., Competition Between Extinction and Enhancement in Surface-Enhanced Raman Spectroscopy **2013** *J. Phys. Chem. Lett*, 4, 1193–1196.

The importance of absorption of the Raman scattered light has been recognized by certain reports.[9] However, they do not describe the necessary link and competition between the enhancement and the extinction. For example, it is commonly known to experimentalists that gold nanospheres exhibit a plasmon resonance at 520 nm and should produce a large local field enhancement when illuminated at 532 nm; yet, no appreciable Raman signal is observed upon 532 nm excitation commonly ascribed to interband transitions in gold.[10] Away from the plasmon resonance frequency maximum, the Raman signal is again observed and actually increases as the excitation wavelength becomes longer.

We address the issue of extinction by a suspension of nanoparticles in SERS experiments through an effective-medium approach. It is shown that extinction and enhancement are tied to each other and compete in such a way that peak signals are acquired off resonance and that, at any wavelength, an optimal particle concentration exists to maximize the Raman signal. We provide verification of the model with experiments in which the particle concentration was varied.

2.2 Theory

Propagation of light in a dilute suspension of identical particles is well-approximated by propagation through a homogeneous medium with an effective refractive index $\tilde{m}$ as described by Bohren and Huffman:[11]

$$\tilde{m} = m\left[1 + i\frac{2\pi\rho}{k^3}S(0)\right] \tag{2.1}$$

where m is the refractive index of the medium in which the particles are embedded, $k = \omega / c$ is the wavenumber in the medium, ρ is the number of particles per unit volume and S(0) is the

scattering amplitude in the forward direction. The absorption coefficient in a medium with complex refractive index is $\alpha = 2k\,\mathrm{Im}\{\tilde{m}\}$. For a suspension with small identical particles the absorption coefficient is given by $\alpha = 4\pi m\rho k^{-2} Re\{S(0)\} = m\rho C_{ext}$, where C_{ext} is the extinction cross section of a single particle in the suspension, proportional to the real part of the forward scattering amplitude. As illustrated in Figure 6(a), the attenuation of a well-collimated beam propagating through the effective medium is described by Beer's law, $I(h) = I(0)\, e^{-hm\rho C_{ext}}$, where I is the field intensity, and h is the propagation distance.

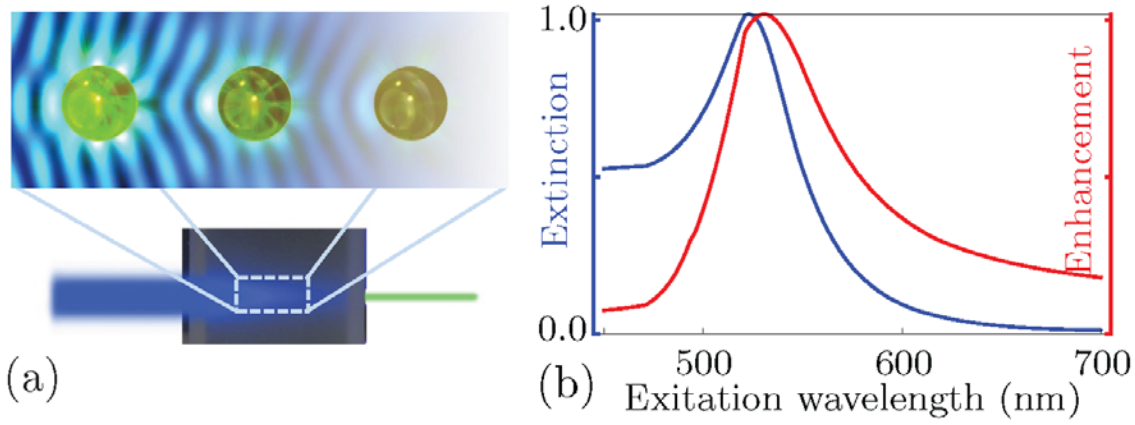

Figure 6. (a) Illustration of two competing mechanisms, where particles provide enhanced fields for Raman scattering and the same particles form an effective medium with corresponding absorption. (b) A graphical representation of the competing physics of extinction and enhancement.

The extinction cross-section, C_{ext}, for a small metallic sphere with radius a, to terms of order $(ka)^4$, is given by the following:[11]

$$C_{ext} = 4k\pi a^3\,\mathrm{Im}\left\{\frac{p^2-1}{p^2+2}\left[1+\frac{(ka)^2}{15}\left(\frac{p^2-1}{p^2+2}\right)\frac{p^2+27p^2+38}{2p^2+3}\right]\right\}+\frac{8}{3}(ka)^4\pi a^2\,\mathrm{Re}\left[\left(\frac{p^2-1}{p^2+2}\right)^2\right] \quad (2.2)$$

where $p = m_s/m$ is the ratio of the refractive index of the material of the spheres, m_s, to that of the refractive index of the medium, m, which both depend on the wavenumber. For dilute suspension, the change in real part of the refractive index of the effective medium from the

background is negligible. The extinction from gold spheres in a suspension is shown in Figure 6 where the extinction peaks near the Frölich frequency $(\lambda_f = 520\,\text{nm})$: for this calculation the optical constants obtained by Johnson and Christy for gold have been used.[12]

The Raman signal, R, from a single, isolated nanoparticle, depends on the incident field amplitude, E_0, the number of Raman-active molecules, N, the local field enhancement, f(**r, ω)**, and the spatial distribution of those molecules. This last point we address through a probability density, which in general will also depend on the number of molecules present, p(**r**, N). Though not explicitly noted, the local enhancement factor is also dependent on the orientation of the incident electric field vector. The number of molecules attached to the nanoparticle may itself be random and given by probability of finding N molecules attached to the particle P_N. A single molecule at **r** is excited by a field with amplitude E_0 f(**r**, ω_0) f(**r**, ω). We assume the Raman signal from each reporter molecule is statistically independent, so the intensities add. The ensemble-averaged Raman signal for a single nanoparticle is thus given by:

$$R = |\chi|^2 \sum_{N=1}^{\infty} N P_N \int d^3r \left| E_0 f(\mathbf{r}, \omega_0) f(\mathbf{r}, \omega) \right|^2 p(\mathbf{r}, N) \tag{2.3}$$

$$R = \langle N \rangle G R^{(0)} \tag{2.4}$$

where $R^{(0)}$ is the Raman signal from one molecule absent the particle, and G is the Raman enhancement factor and generally depends on p(**r**, N) and P_N. For systems in which the particle placement is independent of the number of particles, the sum and the integral may be carried out independently, the sum yielding the average number of molecules $\langle N \rangle$, and the integral resulting in a G independent of the number of molecules.

The enhancement factor for a small sphere of radius a, ($a \ll \lambda$), with a uniform probability of molecule placement over the surface of the sphere, can be calculated in closed form:[13]

$$G(\omega, \omega_0) = \left|[1 + 2g(\omega_0)][1 + 2g(\omega)\right|^2 \tag{2.5}$$

where $g = (p^2 - 1)/(p^2 + 2)$, ω_0 is the frequency of the incident field and ω is the frequency of the Raman-scattered field.

The enhancement calculated by Equation (2.5) is shown in Figure 1 alongside the extinction. It is clear that enhancement and extinction are closely linked and that when the enhancement is strong, the correspondingly strong extinction must be taken into account. The light falling on a single particle is attenuated by propagation through the suspension and arrives with amplitude attenuated by the factor $\exp[-\int_0^z dz'\rho(z')mC_{ext}(\omega_0)/2]$. The local Raman signal is then $\langle N \rangle R^{(0)} G\rho(z) \exp[-\int_0^z dz'\rho(z')mC_{ext}(\omega_0)]$. In transmission mode, this signal must then propagate out through the medium to z = h and the intensity is attenuated by a factor $\exp[-\int_z^h dz'\rho(z')mC_{ext}(\omega)]$. The total signal is a sum over the signal from all particles such that:

$$R = \langle N \rangle A R^{(0)} G \int_0^h dz\rho(z) \exp\left[-\int_0^h dz'\rho(z')mC_{ext}(\omega_0)\right] \exp\left[-\int_z^h dz'\rho(z')mC_{ext}(\omega)\right] \tag{2.6}$$

where A is the integral over the transverse beam profile normalized to peak value, the effective transverse area of the beam. When the concentration $\rho(z)$ does not depend on z, the integrals can be computed in closed form with the result:

$$R = \langle N \rangle A R^{(0)} G \frac{e^{-mC_{ext}(\omega_0)hp} - e^{-mC_{ext}(\omega)hp}}{mC_{ext}(\omega) - mC_{ext}(\omega_0)} \tag{2.7}$$

From this expression it is seen that there are two competing processes that determine the size of the Raman signal: the enhancement, G, and the extinction that results in an exponential decay of the signal. The same processes that increase the enhancement also increase the extinction. The attenuation due to extinction depends not only on the frequency, but also on the concentration of the nanospheres. This is illustrated in Figure 7(a), where it is shown that for increasing concentration the peak of the signal is shifted farther away from the resonant wavelength. This result explains the absence of Raman signal at the plasmon resonance where extinction is so strong that no signal is observed.

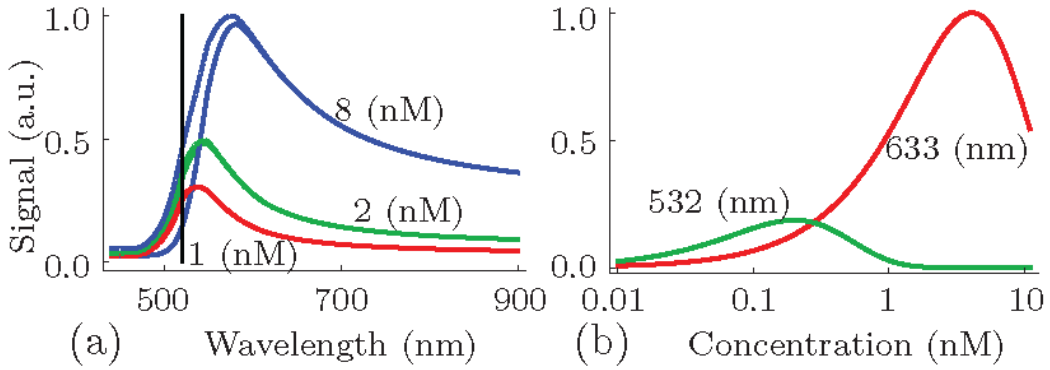

Figure 7. (a) Solid lines: Predicted signal in transmission mode vs. wavelength of the incident light. Reflection mode Raman signal for three different concentrations. The vertical black line indicates the location of the surface plasmon resonance. (b) Transmission mode Raman signal for 532 nm and 633 nm laser excitations. The radius of the spheres is 15 nm.

In reflection mode there is always a contribution from the front layer of the sample which is not attenuated and so the expression for the Raman signal is slightly altered:

$$R = \langle N \rangle A R^{(0)} G \frac{1 - e^{-hm\rho[C_{ext}(\omega) + C_{ext}(\omega_0)]}}{mC_{ext}(\omega) + mC_{ext}(\omega_0)} \tag{2.8}$$

The Raman signal in reflection mode for three different concentrations of nanospheres is shown in Figure 7(a). In reflection mode there is a slightly higher signal due to the blue side of the resonance compared to the signal in transmission mode.

The Raman signal in transmission mode is depicted in Figure 7(b) for two commonly used wavelengths evaluated for a Raman band at 1076 cm^{-1}. For $\lambda = 532\,\text{nm}$, the excitation wavelength is closest to the plasmon resonance, and the signal is very small. A higher signal is found farther away from the resonance with the peak shifted to the red. For relatively low concentrations the largest signal is obtained with a wavelength of 633 nm. Only for concentrations smaller than 0.1 nM is the signal larger for excitation wavelengths closest to resonance. It is seen that there is a concentration that maximized the signal. This optimal concentration can be found by differentiation of Equation (2.8) and equating it to zero:

$$\rho_{opt} = \frac{\ln[C_{ext}(\omega)/C_{ext}(\omega_0)]}{hm[C_{ext}(\omega) - C_{ext}(\omega_0)]} \tag{2.9}$$

when the extinction cross-section, $C_{ext}(\omega)$, equals or is very close to $C_{ext}(\omega_0)$, the optimal concentration becomes $\rho_{opt} = 1/[hmC_{ext}(\omega_0)]$. The strong nonlinearity with concentration that these competing phenomena impose on the recorded signal is also a caution in the development of practical assays and must be taken into account to correctly quantify results across samples. Hence this physics-based analysis enables quantitative molecular imaging for SERS-based microscopy.

2.3 Results and Discussion

The model presented here is validated by measuring the SERS signal of 4,4'-dipyridyl Raman reporter molecules attached to gold nanospheres. Spectra were acquired from the

nanoparticles in suspension using a Raman spectrometer (LabRAM, Horiba) with a 90 second acquisition time. The Raman shift from 200 cm^{-1} to 1800 cm^{-1} was collected at 10 cm^{-1} resolution with 10 mW laser power at the sample. Transmission Raman measurements were collected by focusing laser light through a 1 cm cuvette with a 50 mm focal-length lens and collected with a 100 mm focal-length lens to collimate the transmitted light and direct it to the spectrograph.

Gold nanospheres of 15 nm radius were synthesized by the boiling citrate method. For stability against aggregation, 100 mg of bis(p-sulfonatephenyl)phenylphosphine dehydrate dipotassium salt (BSPP) was added to 100 mL of as-synthesized nanoparticles. The mixture was left to stir overnight (12 – 16 hours) and excess reagents were removed by two centrifugation cycles (3000 RCF, 20 min). For 4,4'-dipyridyl complexation, 1 mL of 10 mM, 4,4'-dipyridyl in water was added to 9 mL of BSPP stabilized gold nanoparticles and left to complex overnight. Excess reagents were removed again by two centrifugation cycles at the same speed. For final purification we dialyzed the solutions in Thermo Scientific G2 Slide-A-Lyzer cassettes against 4 L of nanopure water for 48 hours.

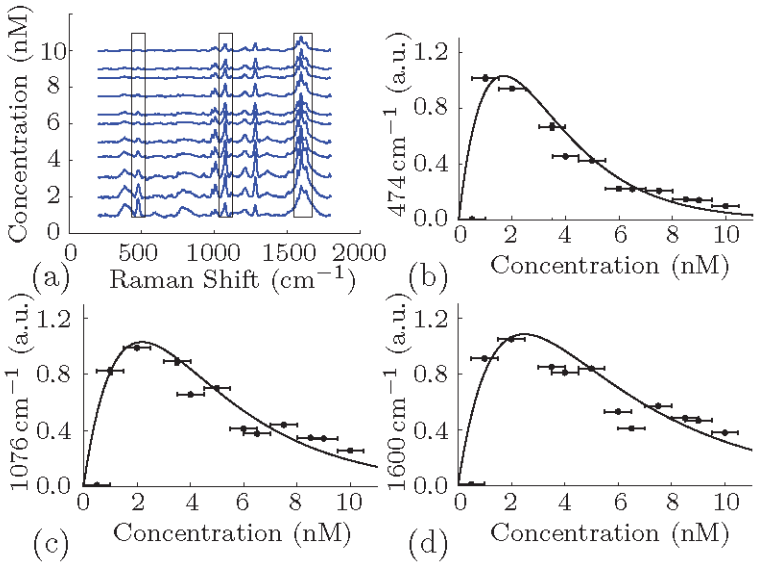

Figure 8. SERS spectra of 4,4'-dipyridyl attached to gold nanospheres with a radius of 15 nm at an excitation wavelength of 633 nm. Measured Raman signals (points) agree with the theoretical prediction (solid line) for a Raman shift of (b) 474 cm^{-1}, (c) 1076 cm^{-1} and (d) 1600 cm^{-1}.

The integrated SERS signal under three different bands (476 cm^{-1}, 1076 cm^{-1}, 1600 cm^{-1}) is compared for different concentrations of gold nanospheres when excited at 632 nm. The SERS spectra from 4,4'-dipyridyl for increasing concentrations is illustrated in Figure 8(a). The three boxes indicate the Raman bands for which the signal is investigated as a function of concentration. The signal is obtained by integration of the Raman band of interest over the width of the box as shown.

As predicted, increasing the concentration of nanoparticles in an attempt to increase the signal leads to signal attenuation beyond an optimal concentration. The measurements are in good agreement with the model. Our results suggest that strategies to increase Raman signals using nanoparticles should not focus on achieving greater local enhancement but instead might strive for designs that maximize total signal by separating the single-particle enhancement and absorption peaks or otherwise tailoring shape of the enhancement and absorption curves to maximize the gap between absorption and enhancement at frequencies away from resonance. A

move towards using thin samples with large areas of collection is also suggested. We see that signal is increased by moving away from resonance and, in some cases, by lowering the concentration of particles. While we focused on nanospheres, our results apply broadly to particle-based Raman enhancement with nonspherical particles as well.

2.4 References

1. Schatz, G. C.; Van Duyne, R. P. *Electromagnetic Mechanism of Surface-enhanced Spectroscopy*; Wiley, 2002; Vol. Volume 1 Theory and Instrumentation.
2. Lyandres, O.; Yuen, J. M.; Shah, N. C.; Van Duyne, R. P.; Walsh, J. T.; Glucksberg, M. R. Progress Toward an In Vivo Surface-Enhanced Raman Spectroscopy Glucose Sensor. *Diabetes Technol Ther* **2008**, *10*, 257–265.
3. Qian, X.; Peng, X.-H.; Ansari, D. O.; Yin-Goen, Q.; Chen, G. Z.; Shin, D. M.; Yang, L.; Young, A. N.; Wang, M. D.; Nie, S. In Vivo Tumor Targeting and Spectroscopic Detection with Surface-enhanced Raman Nanoparticle Tags. *Nat Biotech* **2008**, *26*, 83–90.
4. Von Maltzahn, G.; Centrone, A.; Park, J.-H.; Ramanathan, R.; Sailor, M. J.; Hatton, T. A.; Bhatia, S. N. SERS-Coded Gold Nanorods as a Multifunctional Platform for Densely Multiplexed Near-Infrared Imaging and Photothermal Heating. *Advanced Materials* **2009**, *21*, 3175–3180.
5. Stone, N.; Kerssens, M.; Lloyd, G. R.; Faulds, K.; Graham, D.; Matousek, P. Surface Enhanced Spatially Offset Raman Spectroscopic (SESORS) Imaging – the Next Dimension. *Chem. Sci.* **2011**, *2*, 776–780.
6. Cao, Y. C.; Jin, R.; Mirkin, C. A. Nanoparticles with Raman Spectroscopic Fingerprints for DNA and RNA Detection. *Science* **2002**, *297*, 1536–1540.
7. Talley, C. E.; Jackson, J. B.; Oubre, C.; Grady, N. K.; Hollars, C. W.; Lane, S. M.; Huser, T. R.; Nordlander, P.; Halas, N. J. Surface-Enhanced Raman Scattering from Individual Au Nanoparticles and Nanoparticle Dimer Substrates. *Nano Lett.* **2005**, *5*, 1569–1574.
8. Kodali, A. K.; Llora, X.; Bhargava, R. Optimally Designed Nanolayered Metal-dielectric Particles as Probes for Massively Multiplexed and Ultrasensitive Molecular Assays. *Proceedings of the National Academy of Sciences* **2010**, *107*, 13620 –13625.
9. Maier, S. A. Plasmonic Field Enhancement and SERS in the Effective Mode Volume Picture. *Opt. Express* **2006**, *14*, 1957–1964.
10. Álvarez-Puebla, R. A. Effects of the Excitation Wavelength on the SERS Spectrum. *J. Phys. Chem. Lett.* **2012**, *3*, 857–866.
11. Bohren, C. F.; Huffman, D. R. *Absorption and Scattering of Light by Small Particles*; 2007.
12. Johnson, P. B.; Christy, R. W. Optical Constants of the Noble Metals. *Phys. Rev. B* **1972**, *6*, 4370–4379.
13. Kerker, M.; Wang, D.-S.; Chew, H. Surface Enhanced Raman Scattering (SERS) by Molecules Adsorbed at Spherical Particles: Errata. *Appl. Opt.* **1980**, *19*, 4159–4174.

CHAPTER 3

SURFACE-ENHANCED RAMAN SPECTROSCOPY OF POLYELECTROLYTE-WRAPPED GOLD NANOPARTICLES IN COLLOIDAL SUSPENSION

3.1 Introduction

Plasmonic metal nanoparticles show great promise for biological applications, ranging from diagnostic imaging to *in vivo* therapies.[1-4] Intense electromagnetic fields near the metal surface, which arise from irradiation into the plasmon bands, promote highly sensitive surface-enhanced Raman scattering (SERS), both in substrate-based assays as well as nanoprobes approaching single molecule detection limits.[5] SERS has a dynamic range surpassing that of fluorescence spectroscopy[6] and the ability to multiplex vibrational fingerprints of reporter molecules.[4] The design considerations for such probes focus on maximizing the electromagnetic enhancement defined by their shape, size, and polarization of the incident light.[7] However, there has been great debate in the SERS community regarding the reproducibility and reliability of reported enhancement factors.[8]

Minor differences in synthesis and quantification approaches can produce varying results in the reported SERS enhancement. This is further complicated by sample preparation, such as whether or not the measurements were performed on dried colloidal suspensions, on SERS-active substrates, or on the colloidal suspensions themselves. In previous work we have demonstrated that gold nanocubes dried on gold substrates bearing an analyte monolayer have a higher SERS enhancement compared to gold nanorods prepared in the same way.[9] However, the structures that form as a result of nanoparticle drying have a complicated impact on the resulting signal; aggregation of nanoparticles can create electromagnetic hot-spots. Our understanding of

Reproduced from Sivapalan, S.T., DeVetter, B.M., Yang, T.K., Schulmerich, M.V., Bhargava, R., Murphy, C.J., Surface-enhanced Raman Spectroscopy of Polyelectrolyte-wrapped Gold Nanoparticles in Colloidal Suspension **2013**, submitted.

these effects has rapidly accelerated due to the availability of computational tools based on the discrete dipole approximation (DDA), finite-difference time-domain (FDTD) method, and the finite element method (FEM), among others.[10-12] From simulations, it is well understood that hot-spots are localized areas of high enhancement resulting from interplasmonic coupling between metallic surfaces that may lead to unreliable or difficult-to-reproduce measurements.

In this study we aim to minimize the effects of hotspots by collecting SERS measurements on colloidal suspensions, and using polyelectrolyte-coated nanoparticles to reduce the effect of aggregation. Here, three different geometries (cubes, spheres, trisoctahedra) of gold nanoparticles were synthesized to investigate edge and corner effects. Raman-active reporter molecules trapped near the surface of gold nanoparticles were quantified using electrospray ionization liquid chromatography mass spectrometry (ESI-LC-MS). Additionally, the average number of gold atoms per nanoparticle were quantified via inductively coupled plasma mass spectrometry (ICP-MS). Using these data, we compare SERS signal intensity with a spontaneous Raman calibration curve. Finite element method (FEM) electromagnetic simulations were performed to examine the relationship between the different geometries and the observed SERS signal intensities.

3.2 Experimental Section

Materials. Hydrogen tetrachloride ($HAuCl_4$, > 99.999%), sodium borohydride ($NaBH_4$), polyallylamine hydrochloride (PAH, MW ≈ 15,000 g/mol), polyacrylic acid sodium salt (PAA, MW ≈ 15,000 g/mol, 35 wt. % in H_2O), sodium chloride (NaCl, > 99%), and ascorbic acid ($C_6H_8O_6$, > 99.0%) were obtained from Aldrich and used as received. Cetyltrimethylammonium bromide (CTAB, > 99%) and cetyltrimethylammonium chloride (CTAC, > 98%) were obtained

from Sigma and used without further purification. All glassware were cleaned using aqua regia and rinsed with Barnstead E-Pure 18 MΩ-cm water.

Instrumentation. SERS spectra were obtained on a Horiba LabRAM Raman microscope configured with a 785 nm excitation laser line. Triplicate measurements with integration times of 30 seconds were performed on the gold nanoparticles in suspension through a 1 cm path length quartz cuvette. Laser power at the sample was measured to be 12.5 mW. Zeta potential measurements were performed on a Brookhaven ZetaPALS instrument. Electronic absorption spectra were measured with a Cary 500 scan UV-Vis-NIR spectrophotometer. Transmission electron micrograph (TEM) images were taken on a JEOL 2010F Field Emission Microscope at 200 kV accelerating voltage. For grid preparation 10 μL of gold nanoparticle suspension was drop cast onto holey carbon TEM grids (Pacific Grid-Tech). Size distributions were verified by analyzing at least 100 representative particles per shape. We use a Thermo Scientific Sorvall Legend X1 Centrifuge for purification as detailed in the synthesis below.

Synthesis of seeds for CTAB cubes (A). The nanoparticle seeds were synthesized by modification the method of Nikoobakht and El-Sayed.[13] An aqueous CTAB solution (7.5 mL, 0.1 M) was mixed with 0.25 mL of 0.01 M aqueous $HAuCl_4$. To the stirred solution, 0.6 mL of ice-cold newly-made aqueous 0.01 M $NaBH_4$ was quickly added, which resulted in a light brown solution. After stirring the solution vigorously for 2 minutes, the solution was kept for 1 hour in room temperature before use.

Synthesis of CTAB seeds for trisoctahedra (TOH) gold nanocrystals (B). The nanoparticle seeds were synthesized by following the procedure by Nikoobakht and El-Sayed.[13] An aqueous CTAB solution (7.0 mL, 75 mM) was mixed with 46 μL of 20 mM aqueous $HAuCl_4$. To the

solution, 0.42 mL of ice-cold freshly made aqueous 0.01 M $NaBH_4$ was quickly added under vigorous mixing yielding a light brown solution. After $NaBH_4$ was added, the solution was gently stirred to decompose the excess $NaBH_4$. The solution was used within 2-5 hours after preparation.

Synthesis of CTAB spheres and cubes. Spheres and cubes were synthesized in 40 mL batches. To 32 mL of nanopure water, aqueous solutions of 6.4 mL of 0.1 M CTAB and 0.8 mL of 0.01 M $HAuCl_4$ were added, respectively. This resulted in a yellow-brown solution. Then, 3.8 mL of aqueous 0.1 M ascorbic acid was added as the reducing agent, which rendered the solution colorless. From here depending on the seed concentration, spheres or cubes will form. To obtain spheres, a 0.02 mL of 5 times diluted seed (A) was added to the colorless solution. To obtain cubes, 0.03 mL of 10 times diluted seed (A) was added to the colorless solution. Solutions were allowed to react until no further color changes were observed. The spheres were centrifuged at 4000 rcf for 30 minutes and the supernatant was removed. The pellet was re-suspended in water and this process was repeated again to remove excess CTAB. Similarly, cubes were twice centrifuged at 8000 rpm for 20 minutes.

Synthesis of TOH gold nanocrystals. Trisoctahedra (TOH) nanocrystals were synthesized by a seed mediated method used by Yu et al.[14] A 0.125 mL solution of aqueous 20 mM $HAuCl_4$ was mixed with 9 mL of 22 mM aqueous CTAC. To this mixture, 3.06 mL of aqueous 38.8 mM ascorbic acid was added to make the concentration of ascorbic acid 9.5 mM. The solution was thoroughly mixed. Then, seed (B) was diluted 100 fold with nanopure water, and 50 μL of the diluted seed (B) was added to the solution. This resulted in a red-pinkish solution. Trisoctahedra samples were purified by centrifugation at 4000 rcf for 30 minutes. The supernatant was

discarded and the sample was re-suspended in water. To remove excess CTAC, this process was repeated twice.

Polyelectrolyte wrapping and complexation of methylene blue to gold nanoparticles. To 30 mL of as-synthesized CTAB/CTAC stabilized gold nanoparticles, 6 mL of PAA (10 mg/mL) and 3 mL of NaCl (10 mM) were added and left overnight. Centrifugation and re-suspension into 30 mL of water was performed on each sample to remove excess PAA at the same speeds specified in the synthesis for each shape. To complex the gold nanoparticles with Raman reporter, 1 mL of methylene blue (1 mM) was added to the suspension. After 1 hour, centrifugation was performed again to remove unbound methylene blue. To 30 mL of re-suspended gold nanoparticles, 6 mL of PAH (10 mg/mL) and 3 mL of NaCl (10 mM) was added and left overnight. The samples were again centrifuged to remove excess PAH. Dialysis with 20,000 g/mol dialysis cassettes (Fischer Scientific) was performed for 48 hours in 4 L of water to remove residual reagents. To quantify the number of methylene blue molecules via liquid chromatography mass spectrometry, 1 mL of methylene blue complexed polyelectrolyte wrapped gold nanoparticles were centrifuged into pellets and re-suspended into 50 μL of water. To this suspension, 10 μL of 1 M KCN was added and allowed to sit for at least 1 hour before quantification. The suspension slowly turned colorless as the gold nanoparticles were etched away.

ESI-LC-MS quantification of methylene blue. The LC-MS analysis was performed in Metabolomics Center at UIUC with a 5500 QTRAP mass spectrometer (AB Sciex, Foster City, CA) which is equipped with a 1200 Agilent LC. Analyst (version 1.5.1, Applied Biosytems) was used for data acquisition and processing. An Agilent Zorbax SB-Aq column (5u, 50 x 4.6 mm) was used for the separation. The HPLC flow rate was set at 0.3 mL/min. HPLC mobile phases consisted of A (0.1% formic acid in H_2O) and B (0.1% formic

acid in acetonitrile). The gradient was: 0-1 min, 98% A; 6-10 min, 2% A; 10.5-17 min, 98% A. The autosampler was kept at 5 ºC. The injection volume was 1 µL. The mass spectrometer was operated with positive electrospray ionization. The electrospray voltage was set to 2500 V, the heater was set at 400 ºC, the curtain gas was 35, and GS1 and GS2 were 50, 55, respectively. Quantitative analysis was performed via multiple reaction monitoring (MRM) where m/z 284.2 to m/z 240.1 was monitored.

3.3 Results and Discussion

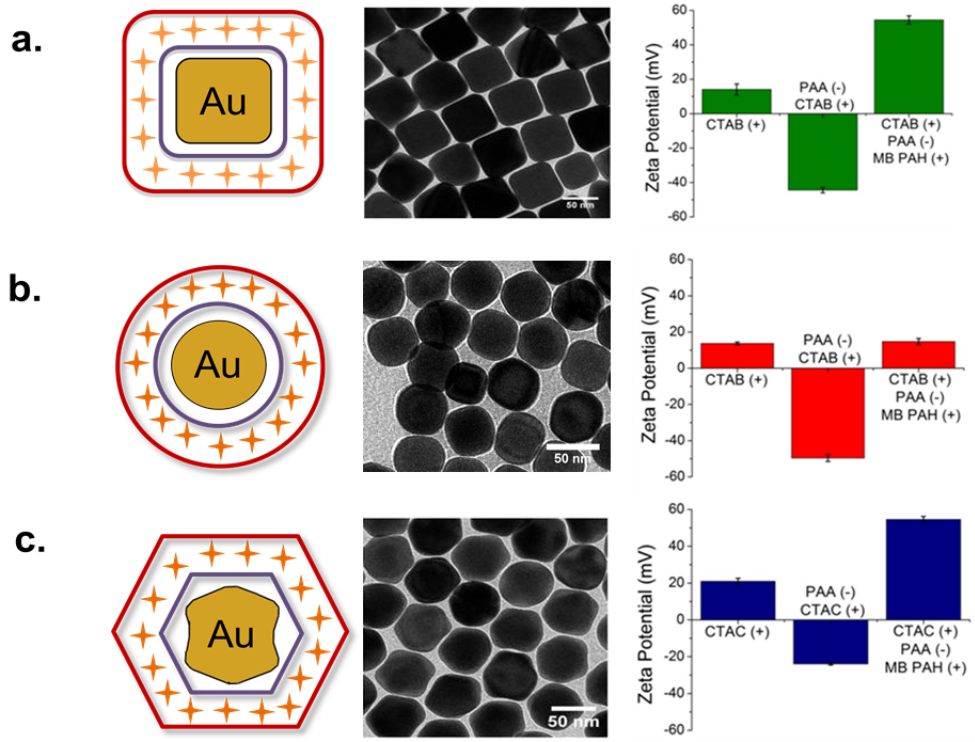

Figure 9. Cartoon illustrating polyelectrolyte trap coating of methylene blue (MB, orange crosses) around gold nanoparticles. MB is electrostatically bound to polyacrylic acid (PAA, purple) and trapped by polyallylamine hydrochloride (PAH, dark red). Transmission electron micrographs of nanoparticle shapes and corresponding zeta potential for (a) cubes (b) spheres and (c) trisoctahedra as a function of wrapping stage.

Polyelectrolyte-wrapped nanoparticles are highly resistant to aggregation and provide a buffering layer of roughly 5 nm from each metallic surface.[15] Raman-active molecules of methylene blue were electrostatically trapped between a layer of anionic polyacrylic acid (PAA) and cationic polyallylamine hydrochloride (PAH). Three nanoparticle geometries (cubes,

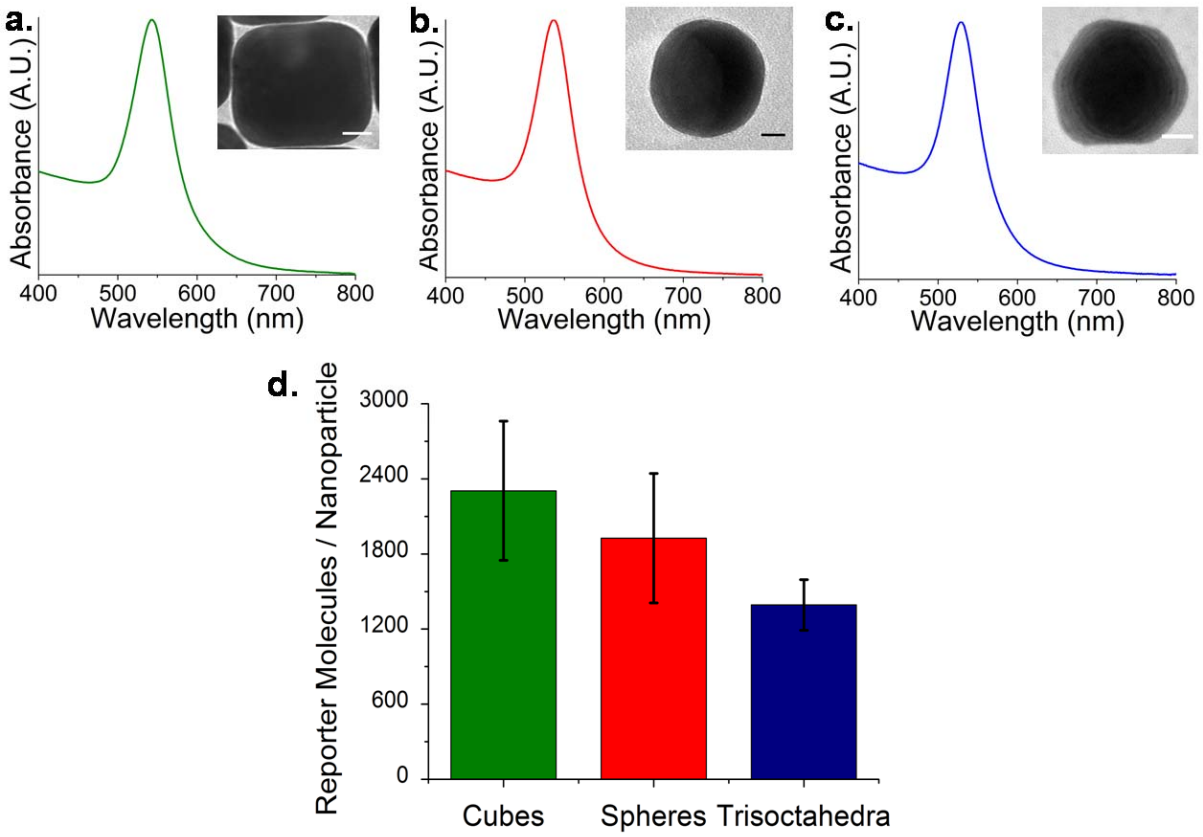

Figure 10. Normalized electronic absorption spectra of colloidal suspensions of (a) cubes, (b) spheres, and (c) trisoctahedra. Inset: transmission electron micrographs of each shape. Scale bars = 10 nm. (d) Experimental ESI-LC-MS quantification of the average number of methylene blue molecules per gold nanoparticle shape. Error bars indicate the standard deviation over four independently synthesized samples.

spheres, and trisoctahedra) with polyelectrolyte layers and trapped methylene blue molecules are depicted in Figure 9 with their corresponding transmission electron micrograph (TEM) images.

Each synthetic step was verified using zeta potential measurements to indicate successful wrapping.

The far-field optical properties of the colloidal suspensions are nearly identical as shown in the experimental electronic absorption spectra (Figure 10). Recently, we have demonstrated a dependence on realized signal for in-suspension measurements due to an interrelationship between localized surface plasmon resonance (LSPR) and laser excitation wavelength.[16] Nanoparticle suspensions were synthesized with similar LSPR maxima in order minimize these effects. Here, four independently synthesized batches of cubes, spheres, and trisoctahedra had LSPR maxima at 543 nm, 537 nm, and 529 nm, respectively, to maximize signal for 785 nm excitation.[16] Characterization with TEM revealed the average size of each shape to be 54.3 ± 3.35 nm, 46.54 ± 6.7 nm, and 52.3 ± 5.8 nm for cubes, spheres, and trisoctahedra, respectively. The average number of reporter molecules (methylene blue) per nanoparticle shape were quantified with ESI-LC-MS against known concentrations of reporter standards (see Experimental Section). On average, there were between 1200 and 2400 molecules per gold nanoparticle. Both experimental[17] and theoretical[18] reports typically assume monolayer coverage of Raman-active molecules. With an assumed molecular profile of 0.66 nm^2/molecule for methylene blue,[19] expected monolayer coverage was over 10,000 molecules per nanoparticle. In all cases, each nanoparticle shape had less than 25% coverage (Figure (10(d)).

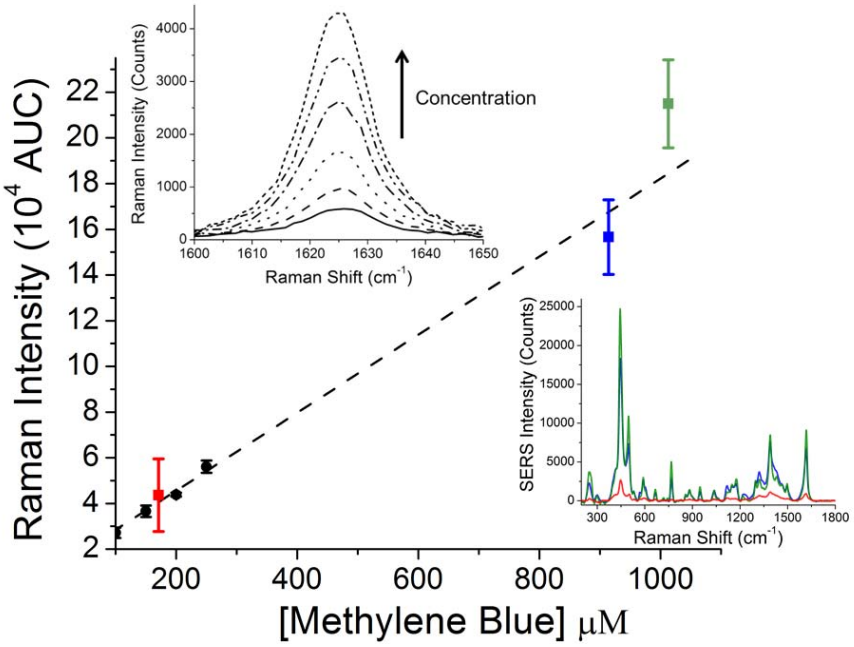

Figure 11. Spontaneous Raman calibration curve of the ~1625 cm^{-1} band of methylene blue (black dots), compared to the same concentration of methylene blue bound to gold nanospheres (red square), gold trisoctahedra (blue square) and gold nanocubes (green square). Error bars correspond to the standard deviation of nanoparticle concentration and reporter molecules per nanoparticle as determined by ICP-MS and ESI-LC-MS, respectively. Top left inset: Spontaneous Raman spectra (between 1600 cm^{-1} and 1650 cm^{-1}) of varying concentrations of methylene blue in water (25 – 400 μM). Bottom right inset: Example spectra calculated from the spontaneous Raman calibration curve with an assumed 0.12 nM gold nanoparticle concentration and 1800 reporter molecules per nanoparticle (cubes, green; trisoctahedra, blue; spheres, red).

Quantitative comparison of SERS data were performed by measuring the spontaneous Raman intensity of methylene blue in water with 25 μM - 400 μM concentrations. All measurements were acquired with exactly the same laser power, acquisition times, and laser configuration used for SERS measurements. From these data, a spontaneous Raman calibration curve was constructed via integration of the band at ~1625 cm^{-1} (Figure 11). Due to conformational changes in the methylene blue molecules during the binding process, the SERS signal intensity was quantified at 1616 cm^{-1}. SERS measurements were performed in aqueous

solution on nanoparticle ensembles at an average concentration of 0.074 nM, 0.12 nM, and 0.17 nM for cubes, spheres, and trisoctahedra, respectively.

Table 1: Observed Raman intensity of each nanoparticle shape. Intensity values were determined from extrapolation of the spontaneous Raman calibration curve of methylene blue with SERS measurements normalized to nanoparticle concentration (determined by ICP-MS) and the average number of reporter molecules per nanoparticle (determined by ESI-LC-MS).

Nanoparticle Shape	Observed Raman Intensity
Cubes	$5.63 \pm 0.56 \times 10^3$
Spheres	$0.87 \pm 0.52 \times 10^3$
Trisoctahedra	$4.01 \pm 0.20 \times 10^3$

An observed Raman intensity (Table 1) may be calculated from extrapolation of the spontaneous Raman calibration curve such that: $\text{Observed Raman Intensity} = \frac{(\text{SERS}_{1616} - 12472)}{157\, N_{conc} M_{molec}}$

where N_{conc} is the average concentration of gold nanoparticles and M_{molec} is the average number of reporter molecules per nanoparticle. The slope m = 157 and the y-intercept b = 12472 were determined from linear regression of the spontaneous calibration curve. The indicated error corresponds to the averaged standard deviation of reporter molecules per sample as determined by ESI-LC-MS. Gold nanocubes have the highest observed intensity of 5.63×10^3.

Nanostructures with high radii of curvature concentrate optical fields through the so-called "lightning rod" effect of SERS.[20] Recent computational studies have emphasized the importance of edge effects in SERS-based measurements.[21, 22] We performed FEM electromagnetic simulations to visualize edge effects on nonspherical geometries. In contrast to other popular techniques such as FDTD and DDA, FEM utilizes adaptive meshes rather than cubic grids subsequently improving near-field accuracy as well as significantly decreasing solver time.[18] All calculations were performed using a commercial software package (COMSOL Multiphysics 4.2). Bulk gold optical constants were obtained from Johnson and Christy.[23]

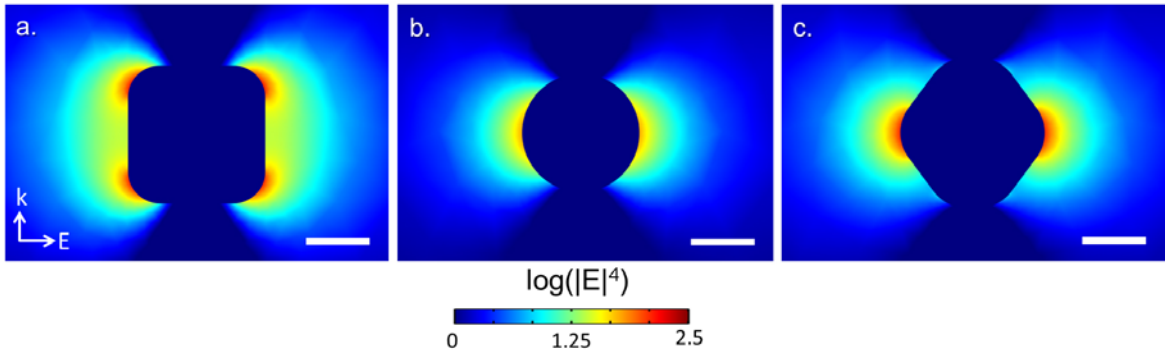

Figure 12. Electric field distributions of single nanoparticle shapes: (a) 54 nm diameter cube, (b) 46 nm diameter sphere, (c) 52 nm diameter trisoctahedra evaluated at λ = 785 nm. Water (n = 1.33) is assumed to be the surrounding media. Scale bar 25 nm.

Cubes, spheres, and trisoctahedra were simulated in a three-dimensional scattering domain. Electromagnetic enhancement is quantified by a factor G where it is assumed that the Stokes' shifted wavelength of Raman scattered light is negligible:

$G = |E(\lambda_{inc})|^2 |E(\lambda_{inc} + \delta\lambda)|^2 \approx |E(\lambda_{inc})|^4$. Assuming submersion in water (n = 1.33), cubes were modeled with an edge length of 54 nm, spheres with a diameter of 46 nm, and trisoctahedra with an effective diameter of 52 nm, corresponding to the average dimensions measured in TEM. Furthermore, we neglect any chemical enhancement effects, as they are expected to be minimal

with our chosen reporter molecule. Corner roundness was empirically determined from TEM image analysis using ImageJ software developed at the National Institutes of Health (Figure 12). As expected from the lightning rod effect, nanostructures with the sharpest corners have the highest enhancement factor G. Despite having more corners, trisoctahedra are relatively smooth as compared to the edges of gold nanocubes.

Surface integration of $|E|^4$ normalized to nanoparticle surface area reveals that cubes have a 2.5x greater field strength as compared to trisoctahedra and spheres. The observed Raman intensity, however, of cubes is over 5x greater than that of spheres. Trisoctahedra have an observed intensity greater than 4x that of spheres. Therefore, we suggest that the primary mechanism of enhancement is due to the lightning rod effect because of the sharp edges and corners that exist on the cubes and trisoctahedra. Differences in the simulated versus experimental data arise from variability in the molecular trap coating process.

The quantitative approach to ensemble SERS measurements presented here demonstrates a novel method to compute observed Raman intensity using a spontaneous Raman calibration curve. In combination with reporter molecule and gold nanoparticle quantification, we have demonstrated that gold nanocubes have the highest SERS signal relative to trisoctahedra and spheres. Trisoctahedra bearing high-index facets such as (221), (331) and (441)[24] are of particular interest due to their increased chemical reactivity.[25] Future work will involve studying the binding density and binding sites available to SERS-active molecules on high-index nanostructures.

3.4 References

1. Boisselier, E.; Astruc, D. Gold Nanoparticles in Nanomedicine: Preparations, Imaging, Diagnostics, Therapies and Toxicity. *Chem. Soc. Rev.* **2009**, 38, 1759-1782.
2. Qian, X. M.; Peng, X. H.; Ansari, D. O.; Yin-Goen, Q.; Chen, G. Z.; Shin, D. M.; Yang, L.; Young, A. N.; Wang, M. D.; Nie, S. M. In Vivo Tumor Targeting and Spectroscopic Detection with Surface-Enhanced Raman Nanoparticle Tags. *Nature Biotechnol.* **2008**, 26, 83-90.
3. von Maltzahn, G.; Park, J. H.; Agrawal, A.; Bandaru, N. K.; Das, S. K.; Sailor, M. J.; Bhatia, S. N. Computationally Guided Photothermal Tumor Therapy Using Long-Circulating Gold Nanorod Antennas. *Cancer Res.* **2009**, 69, 3892-3900.
4. Zavaleta, C. L.; Smith, B. R.; Walton, I.; Doering, W.; Davis, G.; Shojaei, B.; Natan, M. J.; Gambhir, S. S. Multiplexed Imaging of Surface Enhanced Raman Scattering Nanotags in Living Mice Using Noninvasive Raman Spectroscopy. *Proc. Natl. Acad. Sc. U.S.A* **2009**, 106, 13511-13516.
5. Nie, S. M.; Emory, S. R. Probing Single Molecules and Single Nanoparticles by Surface-Enhanced Raman Scattering. *Science* **1997**, 275, 1102-1106.
6. Pieczonka, N. P. W.; Aroca, R. F. Single Molecule Analysis by Surfaced-Enhanced Raman Scattering. *Chem. Soc. Rev.* **2008**, 37, 946-954.
7. Alvarez-Puebla, R. A. Effects of the Excitation Wavelength on the SERS Spectrum. *J. Phys. Chem. Lett.* **2012**, 3, 857-866.
8. Margueritat, J.; Gehan, H.; Grand, J.; Lévi, G.; Aubard, J.; Félidj, N.; Bouhelier, A.; Colas-Des-Francs, G.; Markey, L.; Marco De Lucas, C. et al. Influence of the Number of Nanoparticles on the Enhancement Properties of Surface-Enhanced Raman Scattering Active Area: Sensitivity Versus Repeatability. *ACS Nano* **2011**, 5, 1630–1638.
9. Atkinson, A. L.; McMahon, J. M.; Schatz, G. C. FDTD Studies of Metallic Nanoparticle Systems - Self Organization of Molecular Systems. Russo, N.; Antonchenko, V. Y.; Kryachko, E. S., Eds. Springer Netherlands: 2009; pp 11-32.
10. Jain, P.K.; Lee, K.S.; El-Sayed, I.H.; El-Sayed, M.A. Calculated Absorption and Scattering Properties of Gold Nanoparticles of Different Size, Shape, and Composition: Applications in Biological Imaging and Biomedicine. *J. Phys. Chem. B* **2006**, 110, 7238-7248.
11. Khoury, C. G.; Norton, S. J.; Vo-Dinh, T. Plasmonics of 3-D Nanoshell Dimers Using Multipole Expansion and Finite Element Method. *ACS Nano* **2009**, 3, 2776-2788.
12. Orendorff, C. J.; Gole, A.; Sau, T. K.; Murphy, C. J. Surface-Enhanced Raman Spectroscopy of Self-Assembled Monolayers: Sandwich Architecture and Nanoparticle Shape Dependence. *Anal. Chem.* **2005**, 77, 3261-3266.
13. Nikoobakht, B.; El-Sayed, M. A. Preparation and Growth Mechanism of Gold Nanorods (NRs) Using Seed-Mediated Growth Method. *Chem. Mater.* **2003**, 15, 1957-1962.
14. Yu, Y.; Zhang, Q. B.; Lu, X. M.; Lee, J. Y. Seed-Mediated Synthesis of Monodisperse Concave Trisoctahedral Gold Nanocrystals with Controllable Sizes. *J. Phys. Chem. C* **2010**, 114, 11119-11126.
15. Gole, A.; Murphy, C. J. Polyelectrolyte-Coated Gold Nanorods: Synthesis, Characterization and Immobilization. *Chem. Mater.* **2005**, 17, 1325-1330.

16. Sivapalan, S.T.; DeVetter, B.M.; Yang, T.K., van Dijk, T.; Schulmerich, M.V.; Carney, P.S.; Bhargava, R.; Murphy, C.J. Off-resonance Surface-Enhanced Raman Spectroscopy from Gold Nanorod Suspensions as a Function of Aspect Ratio: Not What We Thought. *ACS Nano* **2013**, in press.
17. Naujok, R. R.; Duevel, R. V.; Corn, R. M. Fluorescence and Fourier-Transform Surface-Enhanced Raman-Scattering Measurements of Methylene-Blue Adsorbed onto a Sulfur-Modified Gold Electrode. *Langmuir* **1993**, 9, 1771-1774.
18. Kerker, M.; Wang, D. S.; Chew, H. Surface Enhanced Raman-Scattering (SERS) by Molecules Adsorbed at Spherical Particles. *Appl. Optic.* **1980**, 19, 4159-4174.
19. Hahner, G.; Marti, A.; Spencer, N. D.; Caseri, W. R. Orientation and Electronic Structure of Methylene Blue on Mica: A Near Edge X-ray Absorption Fine Structure Spectroscopy Study. *J.Chem. Phys.* **1996**, *104*, 7749-7757.
20. Liao, P. F.; Wokaun, A. Lightning Rod Effect in Surface Enhanced Raman Scattering. *The Journal of Chemical Physics* **1982**, *76*, 751–752.
21. Angulo, A. M.; Noguez, C.; Schatz, G. C. Electromagnetic Field Enhancement for Wedge-Shaped Metal Nanostructures. *J. Phys. Chem. Lett.* **2011**, *2*, 1978–1983.
22. Xu, H.; Aizpurua, J.; Käll, M.; Apell, P. Electromagnetic Contributions to Single-molecule Sensitivity in Surface-enhanced Raman Scattering. *Phys. Rev. E* **2000**, *62*, 4318–4324.
23. Johnson, P. B.; Christy, R. W. Optical Constants of Noble Metals. *Phys. Rev. B* **1972**, 6, 4370-4379.
24. Ma, Y.; Kuang, Q.; Jiang, Z.; Xie, Z.; Huang, R.; Zheng, L. Synthesis of Trisoctahedral Gold Nanocrystals with Exposed High-Index Facets by a Facile Chemical Method. *Angew.Chem. Int. Edit.* **2008**, 47, 8901-8904.
25. Zhang, J.; Langilee, M.R.; Personick, M.L.; Zhang, K.; Li, S.; Mirkin, C.A. Concave Cubic Gold Nanocrystals with High-Index Facets. *J. Am. Chem. Soc.* **2010**, 132, 14012-14014.

CHAPTER 4

CONCLUSION

4.1 Conclusion and Outlook

SERS nanoprobes offer high sensitivity and molecular specificity. A current challenge in the SERS community is the lack of reproducible measurements that arise from both a lack of highly reproducible and sensitive probes as well as from an incomplete understanding of electromagnetic interactions in their use.

We approach the design of SERS nanoprobes for in-suspension based measurements using non-aggregated, monodisperse nanoprobes. Optical fields are not generally as concentrated in these configurations; however, they are much more reliable and do not depend on hot-spots to generate the majority of the signal. This provides an opportunity to characterize probes and use them to understand the optical phenomena inherent in their use for living systems. This aspect was discussed in Chapter 2. As discussed in Chapter 3, we apply cationic and anionic alternating layers of polyelectrolytes to minimize aggregation effects and trap Raman-active molecules. This allows for measurements of non-aggregated suspensions. We are currently studying the stability of nanoprobes in biological media such that we are capable of performing long-term measurements for tracking nanoprobes in living environments. Future work will involve using polyelectrolyte and vitrified nanoprobes to investigate *in vitro* imaging and localization of SERS nanoprobes.